JACS
JOURNAL OF THE AMERICAN CHEMICAL SOCIETY
Article
pubs.acs.org/JACS

Ultrafast Dynamics of Photoisomerization and Subsequent Unfolding of an Oligoazobenzene Foldamer

Sabrina Steinwand,[†] Zhilin Yu,[‡,§] Stefan Hecht,*[,‡] and Josef Wachtveitl*[,†]

[†]Institute of Physical and Theoretical Chemistry, Johann Wolfgang Goethe-University, Max-von-Laue-Str. 7, D-60438 Frankfurt, Germany

[‡]Department of Chemistry & IRIS Adlershof, Humboldt-Universität zu Berlin, Brook-Taylor-Str. 2, 12489 Berlin, Germany

Supporting Information

ABSTRACT: Investigating and deciphering the dynamics of photoswitchable foldamers provides a detailed understanding of their photoinduced conformational transitions, resembling similar processes in photoresponsive biomacromolecules. We studied the ultrafast dynamics of the photoisomerization of azobenzene moieties embedded in a foldamer backbone and the resulting conformational helix−coil transition by time-resolved femtosecond/picosecond pump−probe spectroscopy in the visible and infrared region. During $E \rightarrow Z$ photoisomerization of the azobenzenes, the complexity of the photoinduced conformational transition of the pentameric foldamer $\mathbf{10}_5$ is reflected in distinct spectral characteristics and a 2-fold slower decay of the excited-state absorption bands compared to the monomer **M** ($\tau_{4,\text{foldamer}}$ = 20 ps, $\tau_{4,\text{monomer}}$ = 9 ps). Time-resolved IR experiments reveal the vibrational features of the monomer and the foldamer after photoexcitation, with an additional time constant for the foldamer (τ = 150 ps), indicating the initial steps of unfolding of the helical conformation, which are supported by density functional theory calculations. Our results record the overall sequence of photoinduced structural changes in the foldamer, starting from the initial ultrafast isomerization of the azobenzene unit(s) and ending with the complete unfolding on a later time scale. From our experiments, we could gain insight into the coupling of primary photoisomerization events ("cause") and secondary unfolding processes ("effect") in these oligoazobenzene foldamers.

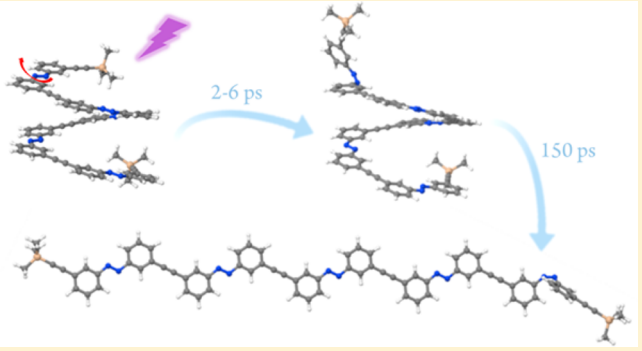

1. INTRODUCTION

Biological macromolecules engage in widespread functions, such as the storage, transcription, and translation of genetic information, the transformation of energy (photosynthesis and respiration), the transduction of signals, and even the formation of the cell membrane.[1] A general prerequiste of these functions is the specific interaction between biopolymers and their substrates, typically involving well-defined, folded conformations. Deciphering the intrinsic conformational dynamics of biopolymers provides a deeper understanding of the underlying mechanism of their biological functions and furthermore allows for the design of artificial soft materials with new and improved properties.

Foldamers are molecules designed to mimic the ability of biopolymers to fold into well-defined structures in solution that are stabilized by forming a number of noncovalent interactions within the locally constrained covalent backbones.[2−5] Depending on the nature of the monomer units, foldamers have proven valuable in various fields, ranging from emulating proteins,[6−8] recognizing DNA,[9] and encapsulating saccharides[10,11] and other small guest molecules[12−14] to optomechanical transduction.[15] Formation of a specific stable helical conformation is also governed by the foldamer's external environment. Typically, varying temperature or solvents induces conformational transitions, occurring with high efficiency due to cooperativity and associated with large structural changes, both of which render foldamers ideal candidates to create stimulus-responsive soft materials with characteristic properties that are governed by the foldamers' conformational dynamics.

In particular, modification of the foldamer backbone with photoswitchable units allows for unprecedented control over the conformational behavior in a noninvasive manner and with exquisite spatiotemporal resolution.[16] For instance, incorporation of azobenzene moieties, which exhibit remarkable structural differences between their *E*- and *Z*-isomers,[17−21] into the backbones of the oligo(*meta*-phenylene ethynylene) (O*m*PE) foldamers[22−28] enables the switching of foldamers between a helical and a random coil conformation upon exposure to UV and visible light.[29−34] The conformational response to an optical stimulus can be enhanced by (i) optimizing the foldamers' chain length[29,33] and the relative orientation[32] of the azobenzene units, (ii) coupling of switching

Received: July 26, 2016
Published: September 6, 2016

DOI: 10.1021/jacs.6b07720
J. Am. Chem. Soc. 2016, 138, 12997−13005

events,[31] and (iii) excitation energy transfer along the backbone to deliberately introduced trap sites.[34]

In general, azobenzene photoswitches can be utilized to remotely control various molecular systems and their associated functions in a wide range of processes, such as the secondary[35,36] or tertiary[37,38] structure of biomacromolecules by covalent incorporation into the backbone of peptides[39] as well as DNA[40,41] and RNA.[42,43] Astonishingly, azobenzenes have been employed in vitro[44] and in vivo.[45,46] However, just as important as the biological use of photoswitches is the use in the context of material science,[47] ranging from liquid crystals[48] and polymers[49] to solar energy storage.[50] In this context, it is important to develop viable strategies to optimize the switching performance of this omnipresent class of photochromic molecules[51] and to integrate them into macro- and supramolecular architectures.[47] The latter requires a detailed understanding of the coupling of the individual switching events in multiswitch constructs, and in this context, foldamers, exhibiting a well-defined three-dimensional structure, have proven very insightful.[52]

Although the thermodynamics and kinetics of the photoinduced $E-Z$ isomerization and subsequent unfolding processes of the oligoazobenzene foldamers have been studied by conventional techniques,[28−32] understanding their interplay and elucidating the resulting conformational dynamics remains a challenge. In the parent O*m*PE foldamers,[22−28] nonexponential kinetics have been observed for the formation of helical conformations in T-jump relaxation measurements.[53] However, incorporating photoswitchable azobenzene moieties in the foldamer backbone provides the unique opportunity to trigger the conformational change at a distinct backbone location with high temporal resolution, enabling dynamic studies by pump−probe experiments.

Herein, we report the dynamics of the helix−coil transition in the amphiphilic oligoazobenzene foldamer $\mathbf{10_5}$, which is composed of five azobenzene units connected in their 3- and 3′-positions via ethynylene linkages and equipped with (chiral) polar oligo(ethylene glycol) side chains (Figure 1).[33] In the

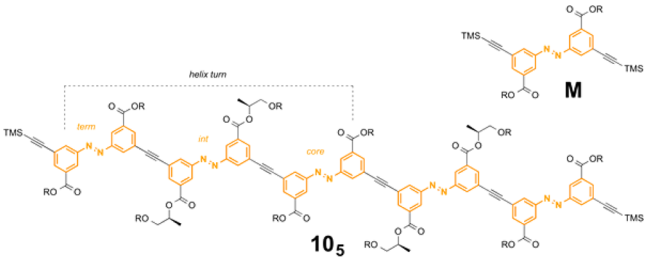

Figure 1. Chemical structures of foldamer $\mathbf{10_5}$ (bottom) and azobenzene monomer unit **M** (top), both in their (all)-*E* configuration (R = $(CH_2CH_2O)_3CH_3$). Three azobenzene units constitute one turn of $\mathbf{10_5}$ in the helical structure (dashed line). The three types of azobenzene units within the foldamer structure are referred to in the text as *core*, *int*, and *term* for the central, internal, and terminal positions, respectively.

polar solvent acetonitrile, the all-*E*-configured foldamer $\mathbf{10_5}$ adopts a helical *cisoid* conformation, which is stabilized by $\pi-\pi$ stacking interactions[54,55] of the aromatic units as well as the solvophobic effect. The photoinduced $E \rightarrow Z$ isomerization of the azobenzenes leads to the quantitative and fully reversible helix−coil transition due to interruption of the $\pi-\pi$ interactions caused by introducing nonplanar *Z*-azobenzene(s). We carried out time-resolved femtosecond/picosecond pump−probe experiments in the visible and infrared region to investigate the dynamics of the $E \rightarrow Z$ photoisomerization mechanism of the azobenzene units and its coupling to the conformational transition of the foldamer. To aid interpretation of the complex conformational dynamics of the foldamer, the isomerization behavior of a respective azobenzene monomer unit **M** (Figure 1) was also studied.

2. RESULTS AND DISCUSSION

Implementation of photoswitches in macromolecules enables their conformation and thus function to be externally controlled with high spatial and temporal precision. For a detailed understanding of the underlying reaction mechanisms, first, the initial dynamics of the light-induced processes of the photoswitch (e.g., photoisomerization of azobenzene) should be determined (see section 2.1). Moreover, an important part is the coupling of the photoswitch to the entire molecule to achieve conformational transduction of the initial photochemical event (see section 2.2). Therefore, to obtain detailed insight into the complete reaction mechanism of the macromolecule upon photoexcitation of the photoswitch, a method is required that can monitor yet distinguish both processes: photoisomerization and subsequent conformational/functional change of the molecule under investigation (see section 2.3). In addition to such time-resolved spectroscopic studies, theoretical modeling of the various reaction pathways of the photoexcited multichromophoric systems provides both validation of the experimental results as well as additional mechanistic insights (see section 2.4).

2.1. Photoisomerization of Azobenzenes as Unfolding Trigger. Azobenzene photoisomerization, which triggers unfolding, is investigated in the UV/vis region for both the azobenzene monomer unit **M** and the foldamer $\mathbf{10_5}$. Besides a reasonable switching behavior, an ultrafast isomerization is desirable to not interfere temporally with the subsequent unfolding process.

The detailed understanding of the isomerization behavior of an individual azobenzene monomer unit is a prerequisite for the characterization of the foldamer $\mathbf{10_5}$. In acetonitrile, the *E*-azobenzene monomer **M** exhibits a $\pi\pi^*$ absorption band at 311 nm and a weak $n\pi^*$ transition at ca. 435 nm (Figure 2). The bands at 250 and 260 nm are attributed to the absorption of the phenylene ethynylene groups.[23,33] Upon exposure to UV light (365 nm), the photoinduced $E \rightarrow Z$ isomerization of the azobenzene monomer **M** takes place, as evident from the gradually decreasing $\pi\pi^*$ absorption band at 311 nm as well as the weakly increasing $n\pi^*$ transition at 425 nm, accompanied by an isosbestic point at 381 nm.[33]

In comparison, the UV/vis spectrum of the all-*E*-azobenzene containing foldamer $\mathbf{10_5}$ is broader and slightly more structured with one main absorption band and one shoulder being observed at 290 and 310 nm. When foldamer $\mathbf{10_5}$ forms a partially stable helical structure in acetonitrile, these two bands correspond to the absorption from the pronounced *cisoid* and the less favorable *transoid* conformation of the phenylene ethynylene backbone.[23,24] Both of these absorption bands overlap with the $\pi\pi^*$ absorption band of the *E*-azobenzenes, leading to a wide absorption range from 320 to 400 nm. In addition, a weak $n\pi^*$ absorption for the azobenzenes appears at 450 nm, around 15 nm red-shifted compared to the monomer. Upon irradiation with UV light (365 nm), the azobenzenes are converted into their metastable *Z*-isomers, as supported by the

DOI: 10.1021/jacs.6b07720
J. Am. Chem. Soc. 2016, 138, 12997−13005

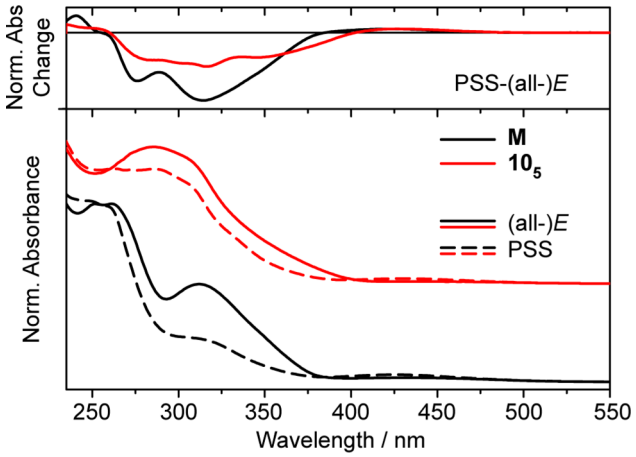

Figure 2. Steady-state UV/vis spectra of the azobenzene monomer unit **M** (4×10^{-5} M) and foldamer **10$_5$** (7×10^{-6} M) in acetonitrile at 25 °C before (in their (all)-*E* configuration, solid line) and after illumination (photostationary state (PSS), dashed line) with 365 nm (bottom) and the corresponding difference spectra in the PSS, normalized to the absorbance difference at 425 nm (top).

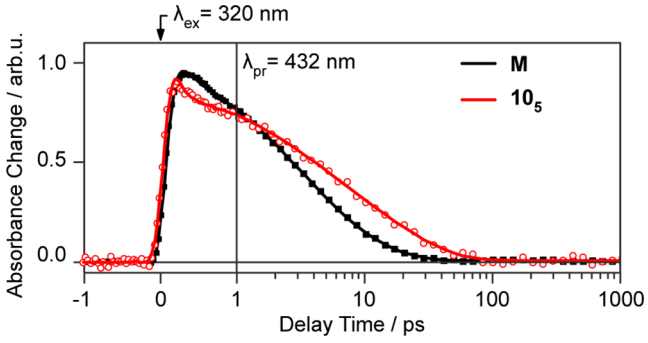

Figure 3. Transients at 432 nm of the azobenzene monomer unit **M** (4×10^{-4} M) and foldamer **10$_5$** (7×10^{-5} M) in acetonitrile at 25 °C after excitation at 320 nm, normalized to the maximum of the absorbance change of each sample around 410 nm.

Table 1. Lifetimes from Global Lifetime Analysis of the Time-Resolved UV-Pump, UV/Vis- and IR-Probe Measurements of Monomer M and Foldamer 10$_5$ upon Excitation at 320 nm

	$E \rightarrow Z$ (λ_{ex} = 320 nm)				
	UV/vis-probe		IR-probe		
lifetime [ps]	**M**	**10$_5$**	**M**	**10$_5$**	lifetime [ps]
τ_1	<0.2	<0.2	*a*	*a*	$\tau_{1'}$
τ_2	0.73	1.69	1.06	1.61	$\tau_{2'}$
τ_3	2.87	5.56	2.80	2.17	$\tau_{3'}$
τ_4	9.09		4.98	8.96	$\tau_{(3,4)*'}$
		20.5	11.5	20.6	$\tau_{4'}$
τ_5	–	nd	–	150	$\tau_{5'}$
τ_6	∞	∞	∞	∞	$\tau_{6'}$

[a]Time resolution of UV/vis-pump IR-probe experiments is ~0.3 ps due to intense coherent artifacts.

decrease of the $\pi\pi^*$ absorption band of the *E*-azobenzene and the increase of the $n\pi^*$ transition band of the *Z*-azobenzene at 425 nm. The isosbestic point is observed at 397 nm and, therefore, is ca. 20 nm red-shifted when compared to the monomer. Due to the occurrence of isomerization events distributed throughout the different embedded azobenzene units as well as the resulting local conformational transitions, a rather heterogeneous mixture of conformations for the foldamer at the photostationary state (PSS) can be assumed, each of which contribute with a slightly different absorbance to the overall absorption spectrum of foldamer **10$_5$** in the PSS. The spectral changes upon irradiation are readily visualized by the difference spectra (Figure 2, top), which show that the photoinduced alteration of the UV/vis absorption of foldamer **10$_5$** spans the entire range from 260 to 400 nm and is significantly broadened compared to the monomer unit. This broad absorption difference is attributed to the collection of conformations adopted by foldamer **10$_5$** in the PSS.

Time-resolved transient absorption measurements were carried out to obtain further insight into the dynamics of the $E \rightarrow Z$ photoisomerization process. For this purpose, the $\pi\pi^*$ absorption band of the *E*-azobenzene moieties in samples of both the azobenzene monomer unit **M** as well as foldamer **10$_5$** was excited at a wavelength of 320 nm (Figure 3). Instantaneously after excitation, two positive excited state absorption (ESA) bands were observed for the monomer in the range between 350 and 650 nm. While ESA$_1$ is located between 350 and 460 nm featured with an intense maximum at 408 nm, the intensity of the ESA$_2$ between 460 and 650 nm with a maximum at ca. 550 nm is moderate (see Figure S1 in the Supporting Information). Four exponential functions are required to satisfactorily describe the global decay of the ESA bands (see Table 1). The decay-associated spectra (DAS; see Figure S2) show that the lifetime τ_1, which is in the range of the time resolution, describes the rise of the ESA bands, in particular, ESA$_1$. Hence, lifetime τ_1 is assigned to the transition from the S$_2$ to the S$_1$ state of the *E*-azobenzene (Figure S2). On the contrary, the lifetimes τ_2, τ_3, and τ_4 describe the decay of the ESA bands. These lifetimes result from the transition from the S$_1$ of the *E*-isomer to the ground state of the *E*-isomer or of the *Z*-azobenzene photoproduct combined with the effect of vibrational cooling. These results are in good agreement with previous studies on the isomerization of azobenzenes.[56−59]

After ~30 ps, the (re)population of the *E*-isomer's and the *Z*-isomer's ground states is complete (Figure 3), as observed in the product absorption (PA) band as well as the ground state bleach (GSB) of the *E*-isomer. An infinite lifetime describes the remaining residues after around 2 ns, which correspond to the contributions of the photoreaction. This spectrum is consistent with the difference spectrum upon steady-state irradiation. Therefore, the photoreaction of monomer **M** is complete within the examined time range, that is, after about 20 ps. In comparison the time-resolved transient absorption, the spectrum of foldamer **10$_5$** exhibits similar general features, such as two ESA bands with a similar location of the maximum and four time constants (see Figure S1). However, while the ESA$_2$ band is quite comparable for both samples, the ESA$_1$ band is significantly broadened for foldamer **10$_5$**, ranging from 350 nm up to ~520 nm with a maximum at 416 nm. This rather broad band is attributed to the complex potential energy surface of foldamer **10$_5$**, resulting from the occurrence of multiple (different) isomerization events of the five azobenzenes within the backbone. This result also clearly shows that more than one of the nonidentical azobenzenes has been excited within the experiment at a given time. Compared to the monomer, the lifetimes of the decays of the absorption bands are significantly prolonged for the foldamer, resulting in lifetimes more than two times larger than the ones for the

DOI: 10.1021/jacs.6b07720
J. Am. Chem. Soc. 2016, 138, 12997−13005

monomer. After approximately 70 ps, the *E*- and *Z*-isomers' ground states of $\mathbf{10}_5$ are completely (re)populated, as evident from the PA band at around 470 nm.

These time-resolved UV-pump UV/vis-probe transient studies confirm that the electronic spectra of the azobenzenes embedded in the backbone of foldamer $\mathbf{10}_5$ show the general features of an azobenzene-type $E \rightarrow Z$ photoisomerization,[56−58] as verified by spectral comparison with the monomer unit **M**. However, the complexity of the overall photoinduced unfolding process in the foldamer, involving multiple, different photoisomerization events and the overlaying conformational transition, is clearly apparent from the broadened spectral absorption bands and the prolonged lifetimes. Therefore, these results clearly demonstrate that the azobenzene photoisomerization plays a critical role in inducing the unfolding process of the foldamer.

2.2. Conformational Transduction from Azobenzene Switch to Foldamer Backbone. To gain further insight into the conformational change of the foldamer upon photoexcitation, steady-state IR experiments were performed to assign the vibrational bands of the foldamer that change upon photoisomerization of the azobenzene trigger.

The steady-state Fourier transform infrared (FTIR) difference spectra (PSS-(all-*E*)) of the monomer and the foldamer show several changes in the vibrational structure located in three separated regions following the $E \rightarrow Z$ photoisomerization (Figure 4). The features between 1320 and 1180 cm^{-1}

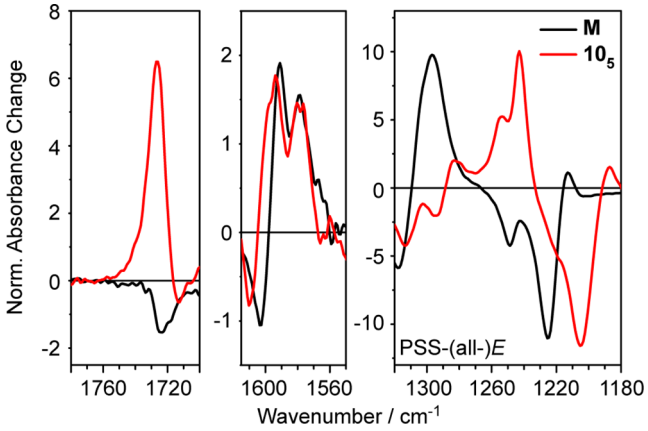

Figure 4. Comparison of FTIR difference spectra of the azobenzene monomer unit **M** (1×10^{-2} M) and the foldamer $\mathbf{10}_5$ (1.6×10^{-3} M) in acetonitrile at 25 °C after illumination with 365 nm (PSS-(all-*E*)). For comparison purposes, spectra were normalized at the absorbance difference maximum of each sample between 1320 and 1220 cm^{-1}.

most likely result from the vibrational changes of the aliphatic groups within the side chains and additional contributions of C−H vibrations of the phenyl rings of the azobenzene backbone (see Figures S7 and S8). In particular, we observe the disappearance of the prominent band of the *E*-isomer at 1225 cm^{-1}, referred to as the in-plane C−H vibration of the aromatic rings, as well as the appearance of a band at 1297 cm^{-1} for the *Z*-isomer, which combines the C−H with the C═O vibrations of the side chains. The carbonyl vibration of the monomer unit **M** within the side chains of the phenyl rings changes only slightly, being more prominent for the *E*-isomer at 1724 cm^{-1} and therefore resulting in a small negative signal, while the foldamer $\mathbf{10}_5$ displays a strong positive band at 1726 cm^{-1}, indicating a more pronouced carbonyl vibration following $E \rightarrow Z$ photoisomerization.

Consequently, we observe significant differences between the monomer and the foldamer in the vibrational region that is diagnostic for the side chains. These vibrational changes couple with both the isomerization events and the unfolding process.

The changes between 1615 and 1550 cm^{-1} are assigned to the vibrations of the aromatic rings, that is, the vibration $\nu_{8a,b}$ of benzene,[60] which is more pronounced for the *Z*-isomer at 1578 and 1591 cm^{-1}. This is in agreement with previous experimental results[60] but also with our density functional theory (DFT) calculations performed in this work (see section 2.4).

For the foldamer, these absorbance changes are attributed to both the photoinduced isomerization events and the conformational transition of the foldamer. Due to the substantial spectral overlap of the contributing aromatic vibrations, it is rather challenging to distinguish the two processes in the steady-state FTIR difference spectra.

2.3. Photoinduced Unfolding Process of the Foldamer. To unambiguously assign these features of the steady-state spectra to either the photoisomerization or the unfolding process, time-resolved UV-pump IR-probe experiments were performed (see Figures S3 and S4). With support from DFT calculations of the vibrational spectra of differently configured foldamers, these experimentally obtained dynamics can be related to the corresponding light-induced unfolding processes.

Upon excitation of the monomer **M** at 320 nm, six dominant GSB bands are observed in the three regions instantaneously following the decrease of the coherent effects at ∼0.3 ps. Most of the GSB bands are consistent with those peaks observed in the FTIR difference spectrum. In addition, several positive absorption difference bands emerge. These bands are associated with both the ESA bands and the absorption of the *Z*-isomers that are formed in the sub-picosecond range characterized by the time constant $\tau_{2'}$. The general dynamics of the absorbance bands is well described by four exponential functions ($\tau_{2'}$, $\tau_{3'}$, $\tau_{(3,4)*'}$, and $\tau_{4'}$), which are in good agreement with the lifetimes of the monomer **M** found in the UV-pump UV/vis-probe experiments (Table 1). However, the lifetime $\tau_{1'}$ cannot be observed due to strong coherent effects up to ca. 0.3 ps. While the lifetimes $\tau_{2'}$ and $\tau_{3'}$ indicate the increase of the ESA bands and the absorption of the *Z*-azobenzene, the lifetimes $\tau_{(3,4)'}$ and $\tau_{4'}$ imply the relaxation and vibrational cooling of these bands. The additional lifetime $\tau_{(3,4)*'}$ is necessary to describe the vibrational cooling satisfactorily. Therefore, a combination of the lifetimes $\tau_{(3,4)*'}$ and $\tau_{4'}$ for the monomer **M** resemble the lifetime τ_4, which stems from the UV/vis-probe measurements. After ca. 50 ps, the ground states of the *E*- and *Z*-isomer are (re)populated, which is slightly longer than estimated from the UV-pump UV/vis-probe experiments (Figures 5 and 6). Afterward, the detected signals in the transient spectra become stable for the monomer, and its signals after ∼2 ns are in quite good agreement with the steady-state FTIR difference spectrum (see Figure S3, right).

The positive bands (ESA) of the monomer **M** show an obvious shift to higher wavenumbers on a time scale up to around 40 ps, which can be described by the four exponential functions quite well (see Figure S5, top). In general, the positive bands of the monomer show a shift of ∼9 cm^{-1} due to the vibrational cooling (at, e.g., 1202 and 1282 cm^{-1}; at 1565 cm^{-1} a shift of ∼17 cm^{-1} can be seen, which is most likely a combination of two bands shifting ∼9 cm^{-1}). We assume a

DOI: 10.1021/jacs.6b07720
J. Am. Chem. Soc. 2016, 138, 12997−13005

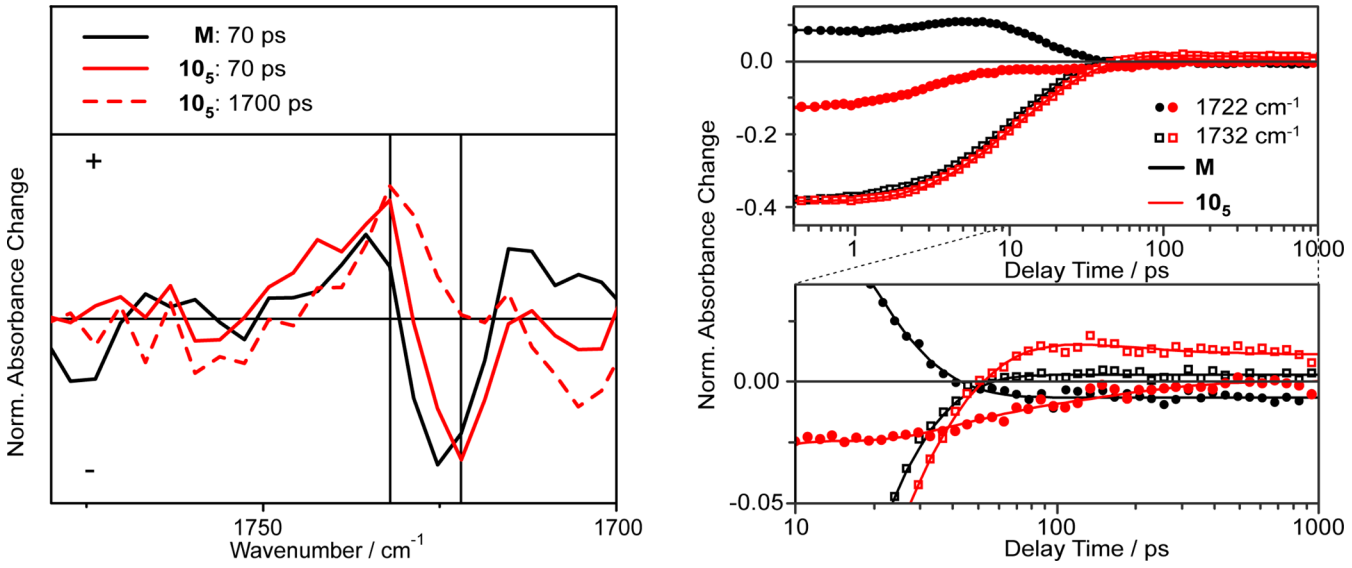

Figure 5. Comparison of time slices of the monomer **M** at a delay time of 70 ps and of the foldamer **10**$_5$ at 70 and 1700 ps, showing the vibrational changes within the carbonyl region (left). Comparison of IR transients of the monomer **M** and the foldamer **10**$_5$ at 1722 and 1732 cm^{-1} after excitation at 320 nm (right, top) and magnified absorbance changes between delay times of 10 to 1000 ps (right, bottom), normalized at the GSB at 0.4 ps at 1732 cm^{-1}. Concentration of **M** and **10**$_5$ is the same as that in Figure 4.

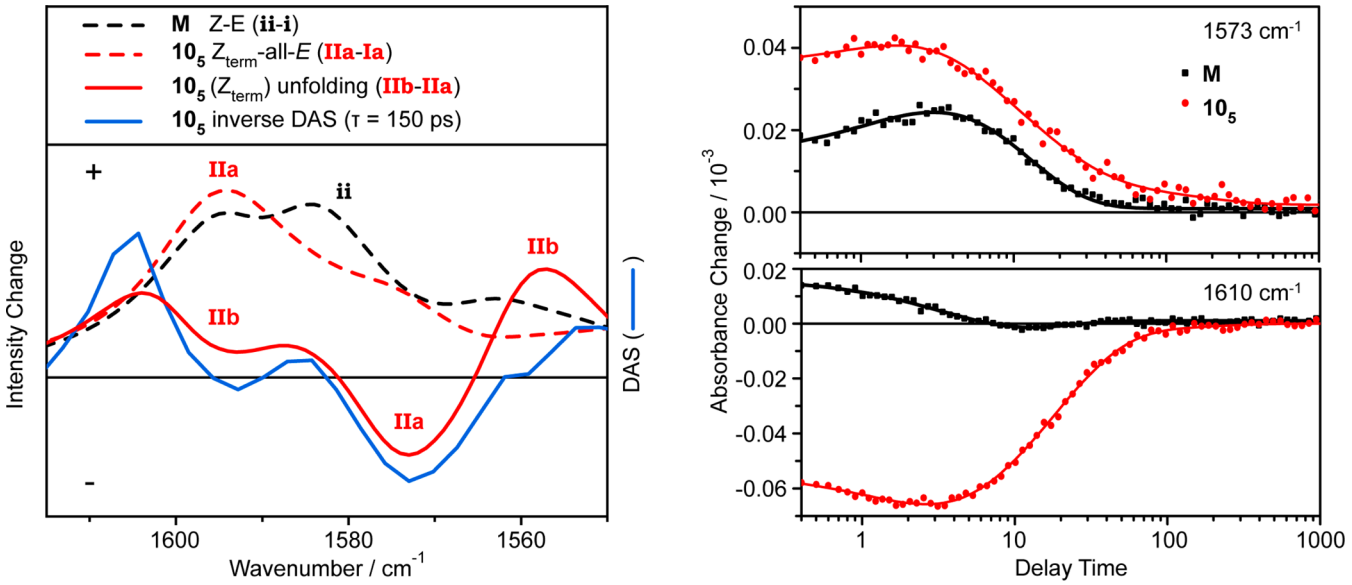

Figure 6. Left: IR spectra were calculated (DFT/B3LYP/cc-PVDZ) for the *E*-**M** (i) and *Z*-**M** (ii), the helical conformation of the all-*E*-**10**$_5$ (Ia), the helical conformation of the foldamer containing one *Z*-isomer at the terminal (IIa) position, and a random coil conformation of the foldamer with one Z_{term}-azobenzene (IIb). The ground-state-optimized structures and the calculated IR spectra are shown in Figures S6 and S9. The photoisomerization of the monomer (with side chains; *Z*-*E*, ii-i) and of the terminal azobenzene of the foldamer **10**$_5$ (without side chains; *Z*-all-*E*, IIa-Ia) can be seen in the difference spectra. The difference between the IR spectra (IIb-IIa) of the foldamer containing one Z_{term}-azobenzene, which is present in a helical conformation (IIa) and in a random coil (IIb), indicates the unfolding of the structured conformation. Also, the similarity of the inverse DAS of τ = 150 ps (blue) and the calculated difference spectrum of the unfolding demonstrates that this time constant describes the rearrangement of the helical conformation after isomerization. Major contributions in the respective difference spectra are indicated by labels. Right: IR transients of the monomer **M** and the foldamer **10**$_5$ at two selected wavenumbers after excitation at 320 nm. At longer delay times, the influence of τ = 150 ps can be seen for the transients of the foldamer **10**$_5$. Concentration of **M** and **10**$_5$ is the same as that in Figure 4.

transfer of the excess energy, which is initially located on one mode, to the coupled bath modes. The transfer of energy highly depends on the displacement factors of this excited vibration and on the coupling of the system. Therefore, it can vary strongly and spread widely over the molecules including the solvent. In earlier studies,[61] a shift of 5 cm^{-1} of the ~1450 cm^{-1} mode (ν_{19} of benzene) was observed, which is significantly smaller than the shift of the monomer shown here. This increased shift can be attributed to the higher anharmonic corrections of ν_8 of benzene (calculated anharmonic corrections (SCF DZP quartic field) ν_8: $(\omega-\nu)_{\text{SCF DZP}}$ = 38 cm^{-1}; ν_{19}: $(\omega-\nu)_{\text{SCF DZP}}$ = 28 cm^{-1}).[62]

Furthermore, regarding the time-resolved IR spectra of foldamer **10**$_5$, this spectral shift of the ESA bands during the cooling process (~6 cm^{-1}) is significantly smaller for the foldamer **10**$_5$ (see Figure S5, bottom). Since the excess energy

DOI: 10.1021/jacs.6b07720
J. Am. Chem. Soc. 2016, 138, 12997−13005

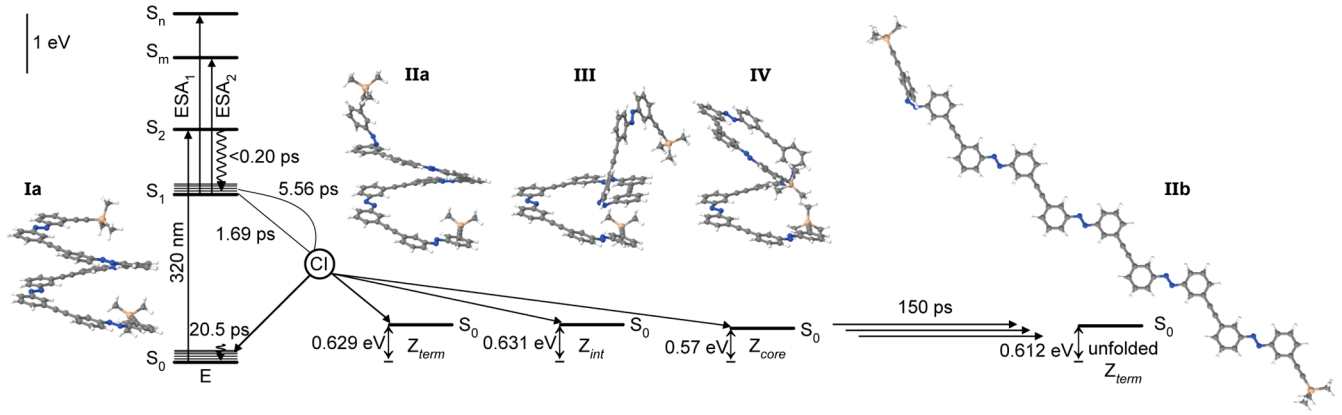

Figure 7. Reaction pathway of the foldamer $\mathbf{10}_5$ in acetonitrile after excitation with UV light in a simplified energy scheme. Chemical structures are ground-state-optimized using DFT/B3LYP/cc-PVDZ and PCM (acetonitrile). Energies from DFT calculations are given relative to the energy of the folded (all)-*E* foldamer $\mathbf{10}_5$. The unfolded structure is feasible for a *Z*-isomer in each position (terminal, internal, and core), however, as shown only for the foldamer containing Z_{term}-azobenzene.

as well as the anharmonic constant should be taken as a constant, this lower shift indicates that a higher number of vibrational modes is used for equilibration in the case of an extended system, which leads to a less pronounced spectral shift. Moreover, the rise as well as the relaxation of the ESA bands can be well described by four time constants. A combination of the lifetimes $\tau_{3'}$ and $\tau_{(3,4)*'}$ for the foldamer $\mathbf{10}_5$ resembles the lifetime τ_3, which results from the UV/vis-probe measurements. Moreover, in particular, lifetime $\tau_{4'}$ reflects the vibrational cooling and matches the lifetime as determined by experiments in the visible region. Interestingly, compared to the transients of the monomer **M**, the foldamer $\mathbf{10}_5$ shows a further kinetic component, which can be described by an additional lifetime of 150 ps (Figure 5, right).

Moreover, in contrast to the results of the monomer, some differences can be obtained for the foldamer by comparison of the time slice after about 1 ns with the steady-state FTIR spectrum, which implies either additional slower conformational changes or an impact of the remaining azobenzenes on the backbone. A comparison of the time slices of the monomer **M** and the foldamer $\mathbf{10}_5$ at a delay time of 70 ps reveals only slight differences in the absorbance changes. Since it is known from the time-resolved UV/vis-pump UV/vis-probe experiments that the isomerization process is finished after about 70 ps, and additionally no differences for the foldamer and the monomer can be observed for the absorbance changes at a delay time of 70 ps, only the photoisomerization process of one azobenzene can be monitored at that delay time. Consequently, absorbance changes after 70 ps, which can be detected for the foldamer $\mathbf{10}_5$ (Figure 5), cannot be assigned to the photoisomerization of the azobenzene anymore. Therefore, these changes in the vibrational structure of the foldamer associated with a lifetime of 150 ps are assigned to an early conformational change, consequently the beginning unfolding of the helical conformation.

2.4. Validation of Unfolding by QM Calculations. To validate the hypothesis of unfolding and to further characterize the vibrational changes, DFT frequency calculations of the monomer as well as the foldamer structures, considering different configurations (*E* vs *Z*) and conformations (helix vs coil), were performed (B3LYP/cc-PVDZ, PCM = acetonitrile). The vibrational change induced by the isomerization of one terminal azobenzene within the foldamer as well as the conformational transition was simulated between 1550 and 1615 cm^{-1} (Figure 6, left; for the difference spectra of foldamer $\mathbf{10}_5$ with a *Z*-azobenzene at the internal and the core positions, see Figure S9). Both processes, the isomerization and the subsequent conformational transition of the foldamer, differ significantly in their contributions within the vibrational structure. While the photoisomerization of the azobenzene results in the rise of several absorption bands associated with the *Z*-isomer, the unfolding of the helical conformation is characterized by a sinusoidal shape of the difference spectrum including positive and negative changes. Comparing the calculated IR difference spectrum of the unfolding with the IR transients (Figure 6, right panel), the small decrease of the absorbance band in the transients of the foldamer at 1573 cm^{-1} at longer delay times and the small increase at 1610 cm^{-1} are in agreement. Regarding the inverse DAS of the lifetime τ = 150 ps, which describes the associated dynamics, the shape of this curve coincides astonishingly well with the calculated IR difference spectrum for the unfolding. Consequently, the unfolding of the helical conformation after photoexcitation starts after about 100 ps.

Since initial conformational changes occur for the foldamer $\mathbf{10}_5$ in the hundreds of picoseconds range, the already mentioned mismatch of some parts of the time slice at a delay time of about 1 ns and the FTIR difference spectrum of the foldamer $\mathbf{10}_5$ indicate that a complete unfolding occurs on a later time scale. However, calculated FTIR difference spectra of the foldamer $\mathbf{10}_5$ containing more than one *Z*-azobenzene (see Figure S9, V-Ia) show that the positive features increase with increasing number of *Z*-azobenzenes, as can also be seen for the experimental FTIR difference spectrum (Figure 4). Therefore, this mismatch is most likely due to a higher degree of isomerization after illumination with LEDs in the steady state. The performed DFT calculations suggest that the foldamer structures resulting after $E \rightarrow Z$ photoisomerization of one azobenzene unit, independent of its position within the backbone, are virtually isoenergetic (Figure 7). A slightly lower energy of a *Z*-isomer in the terminal and core positions can be explained by partially intact helical conformations, which maintain some of the favorable $\pi-\pi$ stacking contacts. However, it cannot be excluded that these structures refer to local energy minima, due to the high number of degrees of freedom. Therefore, each of the three conformations, which

DOI: 10.1021/jacs.6b07720
J. Am. Chem. Soc. 2016, 138, 12997−13005

include a *Z*-isomer at the terminal, the core, or the internal position within the backbone, is feasible after excitation at 320 nm at a delay time below 70 ps. Afterward, the lifetime of 150 ps describes the first conformational change of each of the three possible foldamer structures after the isomerization of one azobenzene (Figure 7, unfolded foldamer structure and its energy level are only shown for the terminal Z_{term}-azobenzene; virtually isoenergetic foldamer structures are expected for each azobenzene position).

3. CONCLUSION

Spectroscopic investigations on the picosecond time scale of the isomerization as well as its influence on the overall structure of the foldamer are inalienable for a gap-free detection of the photoresponsive unfolding of a photoswitchable foldamer. Since little is known about the dynamics of the O*m*PE foldamers, time-resolved UV/vis-pump UV/vis-probe experiments have been performed on the monomer **M** and the foldamer $\mathbf{10}_5$ to study the fast photoisomerization of the azobenzene within the backbone of the foldamer. While, in general, the isomerization mechanisms of the two systems are comparable, the spectra of the foldamer are significantly broadened, as a result of a more complex potential energy surface due to three sterically nonidentical azobenzenes within the backbone and as already evident from the steady-state spectrum. Moreover, the isomerization slows down from the monomer to the foldamer, so the ESA decay time constant of the foldamer is two times higher than that of the monomer. The influence of the $E \rightarrow Z$ photoisomerization on the helical conformation was studied by infrared spectroscopy.

Significant differences between the monomer and the foldamer can be observed in steady-state FTIR experiments in the region of the vibrations located in the side chains of the molecule, which respond to the isomerization process and which are fingerprints of the unfolding process. To differentiate these two processes and to determine their dynamics, time-resolved UV/vis-pump/IR-probe experiments were performed and complemented by DFT calculations (Figure 7). Beside slight spectral differences, the dynamics for the photoisomerization of the monomer and the foldamer do not differ significantly until a delay time of about 70 ps, and only two times higher lifetimes for the vibrational cooling are found for the foldamer, which is in agreement with the measurements in the visible range. After these initial 70 ps, the photoisomerization process is completed for the foldamer as well as for the monomer. However, and in strong contrast to the monomer, subsequent absorbance changes were observed for the foldamer associated with an additional time constant of 150 ps. The corresponding (inverse) decay-associated spectrum, observed experimentally, is in excellent agreement with the calculated IR difference spectrum and describes the unfolding process of the helical conformation after photoisomerization of one azobenzene unit. Our findings suggest that the position of the primary isomerization event, that is, where the initially formed *Z*-azobenzene is located within the backbone of this rather short oligoazobenzene foldamer, has rather little influence on the subsequent unfolding dynamics. From this work, we were able to obtain first detailed insight into how the primary photoisomerization event is coupled to the secondary unfolding process and thereby into the "cause" and "effect" during photoinduced conformational changes in photoswitchable foldamers, mimicking photoresponsive biological macromolecules.

4. EXPERIMENTAL SECTION

4.1. Sample Preparation. Syntheses of the studied azobenzene monomer and foldamer $\mathbf{10}_5$ were reported previously.[33] Both samples were prepared by dissolving the compounds in dry acetonitrile (Sigma-Aldrich). For steady-state UV/vis measurements, about 100 nmol of the monomer unit **M** and about 17.5 nmol of the foldamer $\mathbf{10}_5$ (1.5 mL) were necessary; for time-resolved UV/vis experiments, about 60 nmol of **M** and 10.5 nmol of $\mathbf{10}_5$ (250 μL) were needed, and for the infrared studies, about 350 nmol of **M** and 60 nmol of $\mathbf{10}_5$ (35 μL) were needed. The various concentrations (given in the corresponding figure captions) were chosen to optimize the signal for the different optical path lengths. Steady-state UV/vis measurements were performed in a 1 × 1 cm quartz fluorescence cuvette equipped with a 4 mm stirring bar, allowing simultaneous illumination while measuring. For time-resolved UV/vis studies, a 1 mm quartz cuvette was used. For the infrared studies, the sample was inserted between two CaF_2 windows with a 50 μm Teflon spacer between. At the employed concentrations, aggregation of the foldamer in solution can be excluded.[32,33]

4.2. Experimental Setups. *4.2.1. Steady-State Absorption Measurements.* UV/vis absorption spectra were recorded using a Specord S100 UV/vis spectrometer. FTIR spectra were obtained in a Bruker Vector 22 FTIR spectrometer.

4.2.2. Illumination Procedure. As a light source for illumination, a Thorlabs LED Driver DC4100 and DC4100-HUB was used. $E \rightarrow Z$ photoisomerization was induced by a 365 nm LED and $Z \rightarrow E$ photoisomerization by a 420 nm LED (Thorlabs M365L2 and M420L3). Infrared studies as well as the time-resolved experiments for the $E \rightarrow Z$ photoisomerization were performed by using a Hamamatsu LightningCure spot light source model LC8 (L9588-01 and -04) and a Schott filter combination BG3/GG420 for 420 nm illumination.

4.2.3. Time-Resolved UV/Vis-Pump UV/Vis-Probe Setup. The time-resolved UV/vis transient absorption studies were performed with a CLARK CPA 2001 laser system, with a central wavelength of 775 nm and a pulse duration of 170 fs. It supplied a pulse energy of 800 μJ at a repetition rate of 1 kHz. To achieve the excitation wavelength of 320 nm, two nonlinear processes were necessary. First, a pump pulse with a wavelength of 545 nm was generated in a NOPA. This pulse was then combined with a part of the fundamental laser pulse of 775 nm in a BBO crystal (Θ = 36°), where the sum frequency was generated. At the position of the sample, the resulting pump pulse of 320 nm had a pulse energy of about 70 nJ and a focal diameter of about 170 μm. As a probe pulse, white light was generated in a supercontinuum in a CaF_2 window. This pulse was split into two beams: the signal and the reference pulse. The referenced detection was achieved by two 42-segment diode arrays, which had a resolution of 10^{-4} absorbance units. The instrumental response function was about 200 fs and covered a spectral range from 344 to 650 nm. The sample was kept in a fused silica cuvette with an optical path length of 1 mm, which was moved laterally to ensure the exchange of sample between individual laser shots. The sample concentration was prepared to achieve an optical density of about 0.7 at the excitation wavelength. To exclude effects of anisotropy, the angle between the pump and probe polarization was set to the magic angle (Θ_{ma} = 54.7°).

4.2.4. Time-Resolved UV/Vis-Pump IR-Probe Setup. For the pump pulse, the NOPA was tuned to a central wavelength of 560 nm, which was then combined with a part of the fundamental laser pulse of 775 nm in a BBO crystal. In this sum frequency mixing process, a wavelength of 320 nm was generated. The IR-probe pulse was generated by a two-stage collinear optical parametric amplifier and a following difference frequency of the resulting signal and idler in a $AgGaS_2$ crystal.[63] The resulting IR pulses used in this work ranged from 5.6 to 8.5 μm with a bandwidth >100 cm^{-1}. Both pulses were focused in the same spot in the transversally moved sample. The IR-probe pulse was dispersed in a 250 mm spectrometer (Sure Spectrum 250is, Chromex, Albuquerque, NM) and detected by a liquid-nitrogen-cooled MCT detector. The cross-correlation width was ~0.3 ps.

4.3. Computation. To investigate the influence of photoisomerization and unfolding on the vibrational structure, DFT

DOI: 10.1021/jacs.6b07720
J. Am. Chem. Soc. 2016, 138, 12997−13005

calculations were performed by using the Gaussian 09 package.[64] Geometry optimizations were executed within the polarizable continuum model (PCM)[65] of acetonitrile with a subsequent frequency calculation. The three-parameter hybrid functional of Becke with the correlation functional of Lee, Yang, and Parr (B3LYP) was used.[66,67] Dunning's correlation consistent basis set cc-PVDZ was applied for each calculation.[68] Calculated frequencies were scaled by a factor of 0.97 and overlaid with a Lorentz function of a half-width of 10 cm^{-1}.

■ ASSOCIATED CONTENT

Supporting Information

The Supporting Information is available free of charge on the ACS Publications website at DOI: 10.1021/jacs.6b07720.

Transient absorption difference spectra of the azobenzene monomer **M** and the foldamer $\mathbf{10}_5$ recorded in UV/vis-pump−UV/vis-probe and UV/vis-pump−IR-probe experiments as well as quantum mechanical calculations on the corresponding structures and frequencies (PDF)

■ AUTHOR INFORMATION

Corresponding Authors

*sh@chemie.hu-berlin.de

*wveitl@theochem.uni-frankfurt.de

Present Address

§Department of Chemistry, Northwestern University, 2145 Sheridan Road, Evanston, IL 60208-3108, USA.

Notes

The authors declare no competing financial interest.

■ ACKNOWLEDGMENTS

We thank Dr. Chavdar Slavov for helpful discussions. Generous support by the German Research Foundation (DFG via WA 1850/4-1, SFB 902 "Molecular Principles of RNA-based Regulation", and SFB 765 "Multivalency") as well as the European Research Council (ERC via ERC-2012-STG_308117 "'Light4Function"') is gratefully acknowledged.

■ REFERENCES

(1) Kornyshev, A. A.; Lee, D. J.; Leikin, S.; Wynveen, A. *Rev. Mod. Phys.* **2007**, *79*, 943−996.

(2) Hecht, S.; Huc, I. *Foldamers: Structure, Properties, and Applications*; Wiley-VCH: Weinheim, Germany, 2007.

(3) Hill, D. J.; Mio, M. J.; Prince, R. B.; Hughes, T. S.; Moore, J. S. *Chem. Rev.* **2001**, *101*, 3893−4012.

(4) Guichard, G.; Huc, I. *Chem. Commun.* **2011**, *47*, 5933−5941.

(5) Yashima, E.; Maeda, K.; Iida, H.; Furusho, Y.; Nagai, K. *Chem. Rev.* **2009**, *109*, 6102−6211.

(6) Hayen, A.; Schmitt, M. A.; Ngassa, F. N.; Thomasson, K. A.; Gellman, S. H. *Angew. Chem., Int. Ed.* **2004**, *43*, 505−510.

(7) Horne, W. S.; Gellman, S. H. *Acc. Chem. Res.* **2008**, *41*, 1399−1408.

(8) Guo, L.; Chi, Y.; Almeida, A. M.; Guzei, I. A.; Parker, B. K.; Gellman, S. H. *J. Am. Chem. Soc.* **2009**, *131*, 16018−16020.

(9) Delaurière, L.; Dong, Z.; Laxmi-Reddy, K.; Godde, F.; Toulmé, J.-J.; Huc, I. *Angew. Chem., Int. Ed.* **2012**, *51*, 473−477.

(10) Inouye, M.; Waki, M.; Abe, H. *J. Am. Chem. Soc.* **2004**, *126*, 2022−2027.

(11) Hou, J. L.; Shao, X.-B.; Chen, G. J.; Zhou, Y. X.; Jiang, X. K.; Li, Z. T. *J. Am. Chem. Soc.* **2004**, *126*, 12386−12394.

(12) Tanatani, A.; Mio, M. J.; Moore, J. S. *J. Am. Chem. Soc.* **2001**, *123*, 1792−1793.

(13) Prince, R. B.; Barnes, S. A.; Moore, J. S. *J. Am. Chem. Soc.* **2000**, *122*, 2758−2762.

(14) Garric, J.; Léger, J.-M.; Huc, I. *Angew. Chem., Int. Ed.* **2005**, *44*, 1954−1958.

(15) Bléger, D.; Yu, Z.; Hecht, S. *Chem. Commun.* **2011**, *47*, 12260−12266.

(16) Göstl, R.; Senf, A.; Hecht, S. *Chem. Soc. Rev.* **2014**, *43*, 1982−1996.

(17) Brieke, C.; Rohrbach, F.; Gottschalk, A.; Mayer, G.; Heckel, A. *Angew. Chem., Int. Ed.* **2012**, *51*, 8446−8476.

(18) Beharry, A. A.; Woolley, G. A. *Chem. Soc. Rev.* **2011**, *40*, 4422−4437.

(19) Szymanski, W.; Beierle, J. M.; Kistemaker, H. A. V.; Velema, W. A.; Feringa, B. L. *Chem. Rev.* **2013**, *113*, 6114−6178.

(20) Bandara, H. M. D.; Burdette, S. C. *Chem. Soc. Rev.* **2012**, *41*, 1809−1825.

(21) Abendroth, J. M.; Bushuyev, O. S.; Weiss, P. S.; Barrett, C. J. *ACS Nano* **2015**, *9*, 7746−7768.

(22) Nelson, J. C.; Saven, J. G.; Moore, J. S.; Wolynes, P. G. *Science (Washington, DC, U. S.)* **1997**, *277*, 1793−1796.

(23) Prince, R. B.; Saven, J. G.; Wolynes, P. G.; Moore, J. S. *J. Am. Chem. Soc.* **1999**, *121*, 3114−3121.

(24) Lahiri, S.; Thompson, J. L.; Moore, J. S. *J. Am. Chem. Soc.* **2000**, *122*, 11315−11319.

(25) Brunsveld, L.; Meijer, E. W.; Prince, R. B.; Moore, J. S. *J. Am. Chem. Soc.* **2001**, *123*, 7978−7984.

(26) Matsuda, K.; Stone, M. T.; Moore, J. S. *J. Am. Chem. Soc.* **2002**, *124*, 11836−11837.

(27) Moore, J. S.; Ray, C. R. *Adv. Polym. Sci.* **2005**, *177*, 91−149.

(28) Stone, M. T.; Heemstra, J. M.; Moore, J. S. *Acc. Chem. Res.* **2006**, *39*, 11−20.

(29) Khan, A.; Kaiser, C.; Hecht, S. *Angew. Chem., Int. Ed.* **2006**, *45*, 1878−1881.

(30) Khan, A.; Hecht, S. *Chem. - Eur. J.* **2006**, *12*, 4764−4774.

(31) Yu, Z.; Hecht, S. *Chem. - Eur. J.* **2012**, *18*, 10519−10524.

(32) Yu, Z.; Weidner, S.; Risse, T.; Hecht, S. *Chem. Sci.* **2013**, *4*, 4156−4167.

(33) Yu, Z.; Hecht, S. *Angew. Chem., Int. Ed.* **2011**, *50*, 1640−1643.

(34) Yu, Z.; Hecht, S. *Angew. Chem., Int. Ed.* **2013**, *52*, 13740−13744.

(35) Bredenbeck, J.; Helbing, J.; Sieg, A.; Schrader, T.; Zinth, W.; Renner, C.; Behrendt, R.; Moroder, L.; Wachtveitl, J.; Hamm, P. *Proc. Natl. Acad. Sci. U. S. A.* **2003**, *100*, 6452−6457.

(36) Spörlein, S.; Carstens, H.; Satzger, H.; Renner, C.; Behrendt, R.; Moroder, L.; Tavan, P.; Zinth, W.; Wachtveitl, J. *Proc. Natl. Acad. Sci. U. S. A.* **2002**, *99*, 7998−8002.

(37) Kusebauch, U.; Cadamuro, S. A.; Musiol, H.-J.; Lenz, M. O.; Wachtveitl, J.; Moroder, L.; Renner, C. *Angew. Chem., Int. Ed.* **2006**, *45*, 7015−7018.

(38) Lorenz, L.; Kusebauch, U.; Moroder, L.; Wachtveitl, J. *ChemPhysChem* **2016**, *17*, 1314−1320.

(39) Renner, C.; Moroder, L. *ChemBioChem* **2006**, *7*, 868−878.

(40) Liang, X.; Wakuda, R.; Fujioka, K.; Asanuma, H. *FEBS J.* **2010**, *277*, 1551−1561.

(41) Thevarpadam, J.; Bessi, I.; Binas, O.; Gonçalves, D. P. N.; Slavov, C.; Jonker, H. R. A.; Richter, C.; Wachtveitl, J.; Schwalbe, H.; Heckel, A. *Angew. Chem., Int. Ed.* **2016**, *55*, 2738−2742.

(42) Ito, H.; Liang, X.; Nishioka, H.; Asanuma, H. *Org. Biomol. Chem.* **2010**, *8*, 5519−5524.

(43) Goldau, T.; Murayama, K.; Brieke, C.; Steinwand, S.; Mondal, P.; Biswas, M.; Burghardt, I.; Wachtveitl, J.; Asanuma, H.; Heckel, A. *Chem. - Eur. J.* **2015**, *21*, 2845−2854.

(44) Runtsch, L. S.; Barber, D. M.; Mayer, P.; Groll, M.; Trauner, D.; Broichhagen, J. *Beilstein J. Org. Chem.* **2015**, *11*, 1129−1135.

(45) Wachtveitl, J.; Zumbusch, A. *ChemBioChem* **2011**, *12*, 1169−1170.

(46) Beharry, A. A.; Wong, L.; Tropepe, V.; Woolley, G. A. *Angew. Chem., Int. Ed.* **2011**, *50*, 1325−1327.

(47) Zhao, Y.; Ikeda, T. *Smart Light-Responsive Materials: Azobenzene-Containing Polymers and Liquid Crystals*; John Wiley & Sons, Inc.: New York, 2009.

(48) Garcia-Amorós, J.; Piñol, A.; Finkelmann, H.; Velasco, D. *Org. Lett.* **2011**, *13*, 2282−2285.
(49) Sun, Y.; Wang, Z.; Li, Y.; Zhang, Z.; Zhang, W.; Pan, X.; Zhou, N.; Zhu, X. *Macromol. Rapid Commun.* **2015**, *36*, 1341−1347.
(50) Lennartson, A.; Roffey, A.; Moth-Poulsen, K. *Tetrahedron Lett.* **2015**, *56*, 1457−1465.
(51) Bléger, D.; Hecht, S. *Angew. Chem., Int. Ed.* **2015**, *54*, 11338−11349.
(52) Yu, Z.; Hecht, S. *Chem. Commun.* **2016**, *52*, 6639−6653.
(53) Yang, W. Y.; Prince, R. B.; Sabelko, J.; Moore, J. S.; Gruebele, M. *J. Am. Chem. Soc.* **2000**, *122*, 3248−3249.
(54) Meyer, E. A.; Castellano, R. K.; Diederich, F. *Angew. Chem., Int. Ed.* **2003**, *42*, 1210−1250.
(55) Hunter, C. A.; Lawson, K. R.; Perkins, J.; Urch, C. J. *J. Chem. Soc. Perkin Trans. 2* **2001**, 651−669.
(56) Satzger, H.; Root, C.; Braun, M. *J. Phys. Chem. A* **2004**, *108*, 6265−6271.
(57) Satzger, H.; Spörlein, S.; Root, C.; Wachtveitl, J.; Zinth, W.; Gilch, P. *Chem. Phys. Lett.* **2003**, *372*, 216−223.
(58) Quick, M.; Dobryakov, A. L.; Gerecke, M.; Richter, C.; Berndt, F.; Ioffe, I. N.; Granovsky, A. A.; Mahrwald, R.; Ernsting, N. P.; Kovalenko, S. A. *J. Phys. Chem. B* **2014**, *118*, 8756−8771.
(59) Bahrenburg, J.; Renth, F.; Temps, F.; Plamper, F.; Richtering, W. *Phys. Chem. Chem. Phys.* **2014**, *16*, 11549−11554.
(60) Duarte, L.; Fausto, R.; Reva, I. *Phys. Chem. Chem. Phys.* **2014**, *16*, 16919−16930.
(61) Hamm, P.; Ohline, S. M.; Zinth, W. *J. Chem. Phys.* **1997**, *106*, 519−529.
(62) Maslen, P. E.; Handy, N. C.; Amos, R. D.; Jayatilaka, D. *J. Chem. Phys.* **1992**, *97*, 4233.
(63) Hamm, P.; Kaindl, R. A.; Stenger, J. *Opt. Lett.* **2000**, *25*, 1798−1800.
(64) Frisch, M. J.; Trucks, G. W.; Schlegel, H. B.; Scuseria, G. E.; Robb, M. A.; Cheeseman, J. R.; Montgomery, J. A., Jr.; Vreven, T.; Kudin, K. N.; Burant, J. C.; Millam, J. M.; Iyengar, S. S.; Tomasi, J.; Barone, V.; Mennucci, B.; Cossi, M.; Scalmani, G.; Rega, N.; Petersson, G. A.; Nakatsuji, H.; Hada, M.; Ehara, M.; Toyota, K.; Fukuda, R.; Hasegawa, J.; Ishida, M.; Nakajima, T.; Honda, Y.; Kitao, O.; Nakai, H.; Klene, M.; Li, X.; Knox, J. E.; Hratchian, H. P.; Cross, J. B.; Bakken, V.; Adamo, C.; Jaramillo, J.; Gomperts, R.; Stratmann, R. E.; Yazyev, O.; Austin, A. J.; Cammi, R.; Pomelli, C.; Ochterski, J. W.; Ayala, P. Y.; Morokuma, K.; Voth, G. A.; Salvador, P.; Dannenberg, J. J.; Zakrzewski, V. G.; Dapprich, S.; Daniels, A. D.; Strain, M. C.; Farkas, O.; Malick, D. K.; Rabuck, A. D.; Raghavachari, K.; Foresman, J. B.; Ortiz, J. V.; Cui, Q.; Baboul, A. G.; Clifford, S.; Cioslowski, J.; Stefanov, B. B.; Liu, G.; Liashenko, A.; Piskorz, P.; Komaromi, I.; Martin, R. L.; Fox, D. J.; Keith, T.; Al-Laham, M. A.; Peng, C. Y.; Nanayakkara, A.; Challacombe, M.; Gill, P. M. W.; Johnson, B.; Chen, W.; Wong, M. W.; Gonzalez, C.; Pople, J. A. *Gaussian 09*, revision D.01; Gaussian, Inc.: Wallingford, CT, 2009.
(65) Miertus, S.; Scrocco, E.; Tomasi, J. *Chem. Phys.* **1981**, *55*, 117−129.
(66) Becke, A. D. *J. Chem. Phys.* **1993**, *98*, 5648−5652.
(67) Lee, C.; Yang, W.; Parr, R. *Phys. Rev. B: Condens. Matter Mater. Phys.* **1988**, *37*, 785−789.
(68) Dunning, T. H. J. *J. Chem. Phys.* **1989**, *90*, 1007−1023.

DOI: 10.1021/jacs.6b07720
J. Am. Chem. Soc. 2016, 138, 12997−13005